ELSEVIER

Journal of Nuclear Materials 252 (1998) 110–120

journal of nuclear materials

Modeling of chemical interactions of fuel rod materials at high temperatures
II. Investigation of downward relocation of molten materials

M.S. Veshchunov *, A.V. Palagin

Nuclear Safety Institute (IBRAE), Russian Academy of Science, B. Tulskaya, 52, Moscow 113191, Russia

Received 5 May 1997; accepted 4 September 1997

Abstract

In Part II of the modeling of chemical interactions of fuel rod materials at high temperatures, qualitative results on the nature of Zr-rich melt oxidation and interactions with fuel rods allow further interpretation of the post-test examinations of structures (debris) formed in the CORA tests under more complicated conditions, namely during downward relocation of the melt. In this situation, the molten mass extensively oxidizes and simultaneously dissolves UO_2 pellets and ZrO_2 scales of the cladding. The analysis of these simultaneous physico-chemical processes on the basis of the kinetic oxidation/dissolution model developed in Part I of the paper, allows a new interpretation and explanation of the CORA tests results concerning relocation dynamics of the major part of the melt (slow relocation of melt in the form of massive slug rather than quick relocations of droplets and rivulets), formation of local blockages (debris) in the interrod space and accumulation of the melt in the core region in the form of molten pool. © 1998 Elsevier Science B.V.

1. Introduction

A recently published report on in-vessel core degradation in LWR severe accidents [1] updates to 1995 the original state-of-the-art report in this area released in 1991 [2], and concludes with the identification of the remaining requirements for both model development and experimental work, followed by the main conclusions and recommendations. These conclusions with respect to modeling of core degradation phenomena and development of numerical codes, were completely confirmed by the results of the International Standard Problem ISP36 published in a Comparison Report [3].

It was generally concluded in Refs. [1–3] that the confidence in code predictions decreases with progressing core damage. Entering into the late phase melt progression marked by the onset of substantial formation and relocation of ceramic materials, the level of uncertainty becomes larger. This includes the transition between early and late phase core degradation sequences governed by phenomena like oxidation of complex material mixtures and melts. Melt oxidation models – so far available, see Ref. [3] – are thoroughly based on rate equations for intact rods. In these models rivulets, droplets or films of the (Zr, U, O) melt relocating with a high velocity are considered, and their oxidation kinetics are described by (renormalized) standard parabolic correlations measured in isothermal tests on solid Zircaloy (Zry) cladding oxidation and extrapolated to temperatures above the Zry melting point. Such an approach seems to be oversimplified and inadequate for several reasons:

- The oxidation kinetics of the (Zr, U, O) melt obey essentially more complicated kinetic laws taking into account simultaneous processes of dissolution by the melt of UO_2 fuel pellets and ZrO_2 cladding scales which are competitive to the oxidation process and are accompanied by precipitation of the (U, Zr)O_{2-x} ceramic phase (see Part 1);
- The relocation velocities of visually observed droplets and rivulets are so high ($v \simeq 0.5$ m/s) that the real times

* Corresponding author. Tel.: +7-095 952 2421; fax: +7-095 958 0040; e-mail: vms@ibrae.ac.ru.

PII S0022-3115(97)00284-5

of their interactions with steam (during their relocations) turn to be negligibly small (several seconds!).

Further analysis of post-test examination data of the CORA-W1 and CORA-W2 experiments is presented in the present Part II of the paper in order to reveal mechanisms of relocating materials oxidation. From the comparison of time behavior of high-temperature curves with visual observations of melt propagation fronts, on the one hand, and from the results of metallographic examinations of the solidified blockages in the bundles, on the other hand, it is concluded that the major part of molten cladding material relocates downward, in the form of a massive slug, very slowly in comparison with rather quick relocations of separate drops and rivulets. During this slow downward propagation of the slug, it accumulates fresh portions of melting cladding, extensively oxidizes and simultaneously dissolves UO_2 pellets and ZrO_2 scales of the cladding. The analysis of these simultaneous physico-chemical processes by the kinetic oxidation/dissolution model developed in Part I of the paper allows the explanation of reasons for the observed rather low velocity of slug relocation (owing to the precipitation of the ceramic (U, Zr)O_{2-x} phase in the course of the oxidation/dissolution process) and rather high heat generation provided cladding fusion and heating of the surrounding materials in the course of slug relocation.

2. Qualitative consideration

Detailed analysis of the experimental data obtained in the CORA tests [4] apparently demonstrates that a real behavior of molten materials qualitatively differs from the considerations of the simplified models. As seen from Fig. 1 taken from [5], high and low temperature regions observed at $t \geq 4200$ s in the CORA-W1 test are separated by a rather pronounced temperature front. This front relocates downward with a characteristic velocity $v_1 \simeq 1$–2 mm/s which is extremely small in comparison to the above indicated velocities of rivulets and droplets ($v_2 \simeq 0.5$ m/s). A coincidence of the temperature front with a blockage position in the end of the relocation process (at $t \approx 4800$ s, when electrical heating of rod simulators and steam flux were switched off, leading to quick cooling of the system), was recently confirmed by an additional analysis of material distribution in all the CORA tests [6] and allows some qualitative conclusions. It can be apparently proposed that in the steady stage of the process a slow relocation (with the characteristic velocity $v_1 \simeq 1$–2 mm/s) of a large molten mass occurs at $T \approx 2000$°C slightly above the melting temperature of α-Zr(O) ($T_m \approx 1950$°C). Owing to a large temperature gradient below the front (estimated from Fig. 1 as $\nabla T \approx 50$–80 K/cm), some kind of a refrozen crust forms in the lower part of the melt

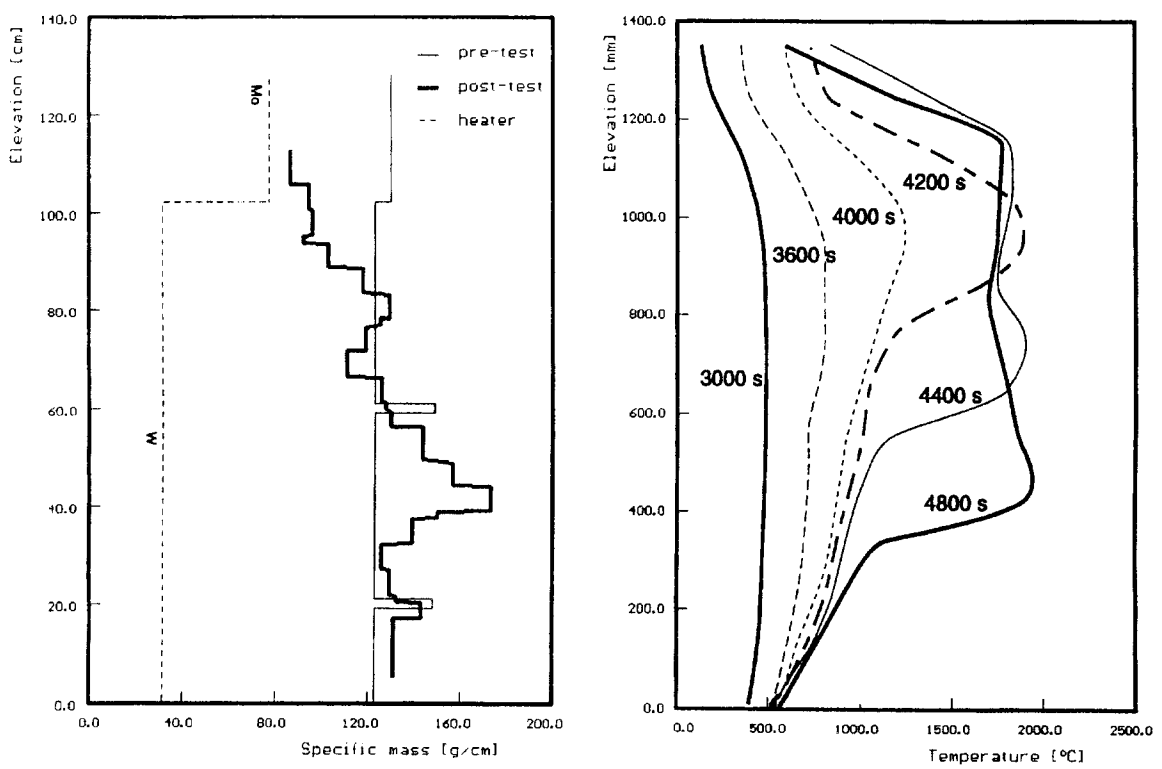

Fig. 1. Axial mass distribution after the test and axial temperature distribution during the transient of test CORA-W1 (from Ref. [5]).

(see below) and prevents the molten mass from quick relocation. Separate droplets and rivulets splash out from the molten mass and/or locally melt through the crust and then quickly relocate downward with their characteristic velocity $v_2 \simeq 0.5$ m/s until they refreeze very soon due to a large temperature drop in the vicinity of the melt progression front.

Visual observations of the CORA test systematized in

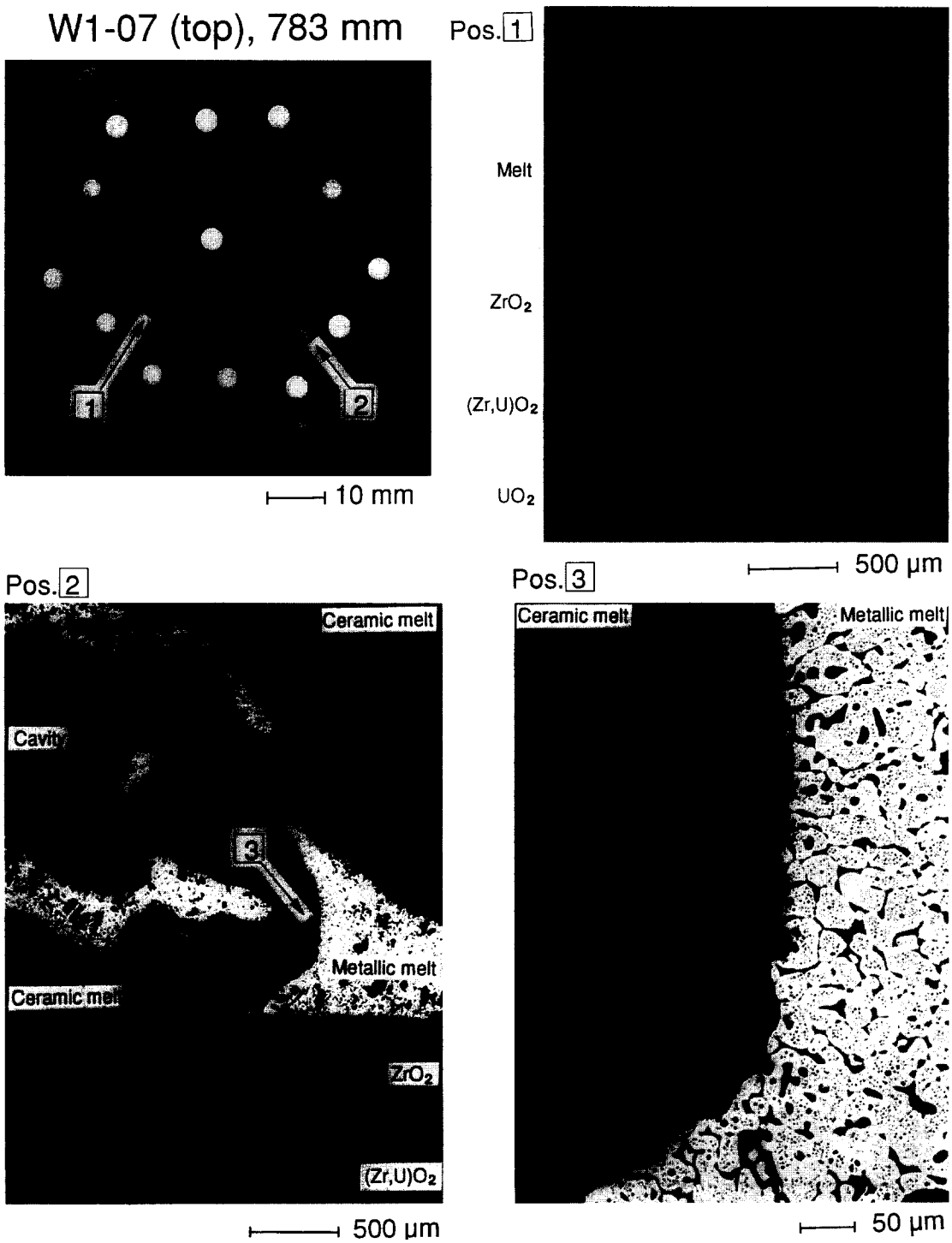

Fig. 2. Cross-section W1-07 (top) of the CORA-W1 test bundle (elevation 783 mm) (from Ref. [5]).

[7] qualitatively confirm the above derived conclusions about the behavior of the melt. Indeed, analysis of practically all the CORA tests show the existence of a 'flamefront' which relocates coherently either with a 'front' of rivulets or with the Zr melting isotherm, and fairly associates with the melt progression front in Fig. 1.

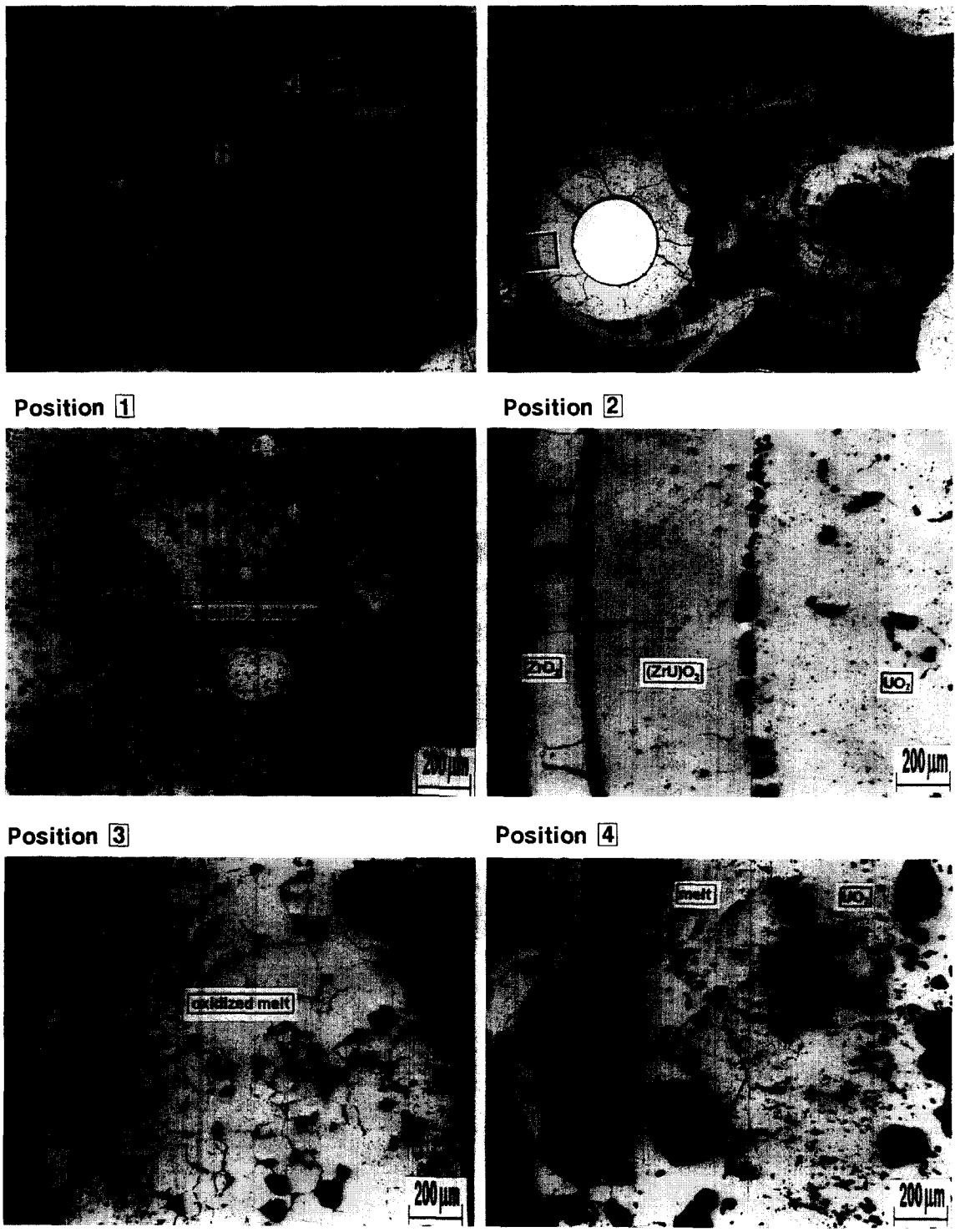

Fig. 3. Oxidized melt microstructures (from Ref. [10]).

Owing to a high difference between the velocities of the molten mass and its separate fragments (rivulets and droplets), $v_2/v_1 \approx 500$, each unit element of the melt spends the most part of the time (t_1) inside the molten mass and only a negligibly small part of time (t_2) inside quickly relocating rivulets or droplets ($t_1/t_2 \approx v_2/v_1 \approx 500$). For this reason, it is clear that interactions with steam are mainly connected with oxidation of the molten mass rather than of separate rivulets and droplets. For the description of this process an additional analysis of available post-test examinations of the samples obtained in the CORA experiments is necessary.

3. Analysis of the CORA post-test examination data

For the analysis of the CORA post-test examination results, the CORA-W1 test is chosen for two reasons:

- being one of the last tests in the CORA series, it is better studied and described in more detail;
- in the absence of absorber rods which have rather low melting temperatures (in the case of (Ag, In, Cd) absorber material) or form low-temperature eutectics with other construction materials (B_4C/Zry or B_4C/stainless steel), the analysis of Zr cladding melt behavior can be performed more unambiguously.

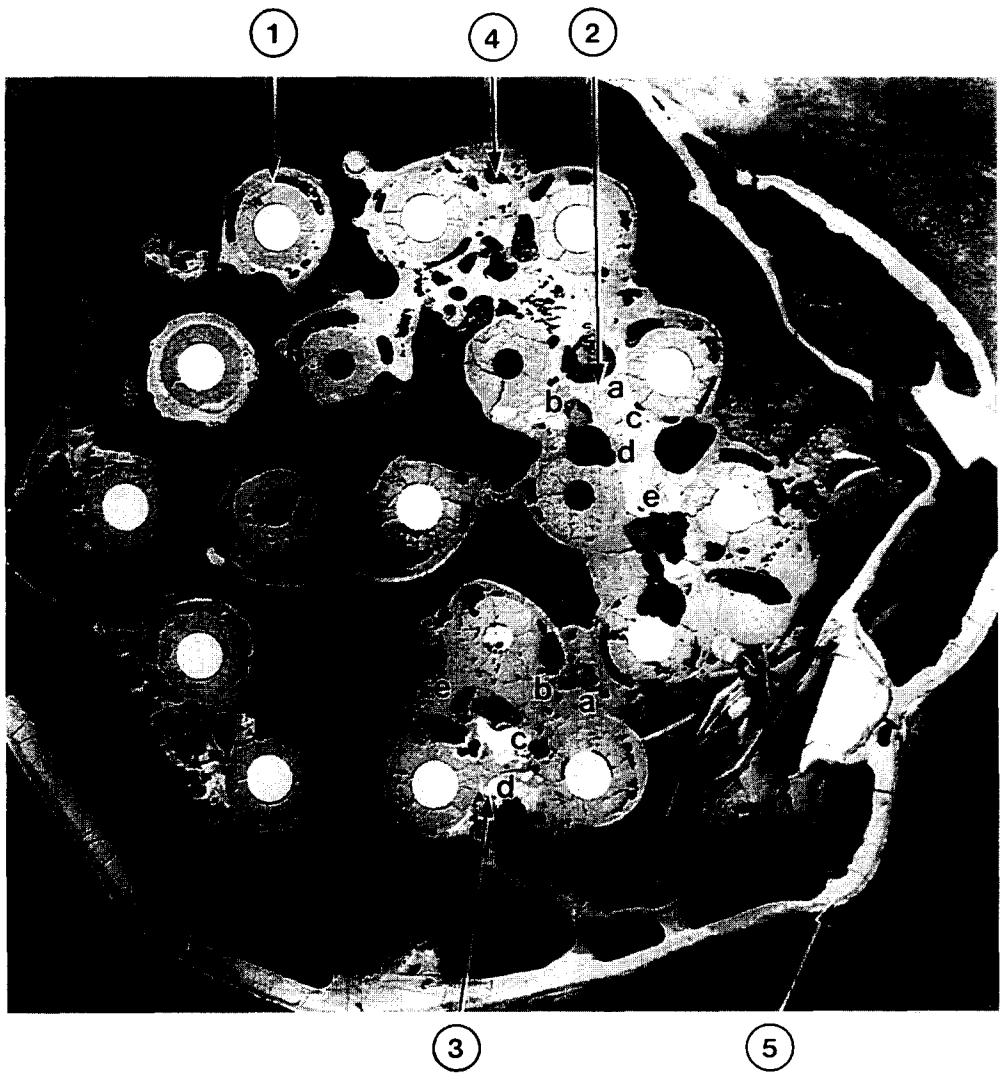

Fig. 4. Cross-section #k of the CORA-W2 test bundle (elevation 605 mm) (from [10]). Positions of SEM/EDX analysis.

Usually it is rather difficult to restore a qualitative picture of material interactions and behavior at high temperatures on the basis of post-test examinations; however, some of these data are rather helpful and straightforward for the description of the high-temperature processes. Among the numerous data of CORA-W1 post-test examinations [5] there are several especially significant and elucidating observations.

(1) As seen from the time–temperature curves analysis (Fig. 1), melting of the Zr cladding and subsequent melt relocations initially occur at the elevation 1000 mm in the CORA-W1 test. From the analysis of bundle post-test cross-sections at different elevations (see fig. 110 in Ref. [5])) it is clearly seen that the first partial blockages are formed already at elevations of 800–900 mm. These observations indicate that after a short initial time interval when the melt appears and relocates in the form of droplets and rivulets, the molten material rather soon accumulates inside the interrod space of various groups of rods and forms some kind of a molten pool in this region. This pool slowly relocates downward (as discussed above) and simultaneously expands laterally due to accumulation of fresh portions of molten cladding. For this reason, a blockage located at a lower elevation ≈ 600 mm fills the essential part of the bundle cross-section (see fig. 111 in Ref. [5]).

(2) In the upper part of the bundle the solidified material consists mainly of the (U, Zr)O_{2-x} ceramic phase alternated with undissolved remnants of ZrO_2 scales and relatively small areas of the refrozen metallic melt (Figs. 2 and 3). The formation of relatively large and uniform areas of the (U, Zr)O_{2-x} ceramic phase can be unambiguously interpreted as a result of precipitation from the oversaturated liquid phase in the course of melt oxidation and simultaneous dissolution of ZrO_2 and UO_2 by the melt at $T \approx 2000$°C (see Part I). This conclusion is based on the observations (see, for example, Ref. [8]) that the liquid metal (Zr, U, O) phase (without ceramic precipitates) always decomposes on the cooling-down to a homogeneous mixture of the α-Zr(O) phase with a relatively small portion of dendritic ceramic particles (compare with point 4 below) which can be easily distinguished visually from the structure presented in Figs. 2 and 3.

(3) Results of point analysis of the chemical composition of the uniform areas of the (U, Zr)O_{2-x} ceramic phase precipitated and grown up in the course of high-temperature interactions of the melt and accumulated in the interrod space of the bundle upper part, are presented in greater detail in the CORA-W2 test (with B_4C absorber rod) [9,10]. In some spatial locations where the influence of B_4C on the melt composition is negligible, the structure of the ceramic blockages is completely identical to that observed in the CORA-W1 tests (Fig. 4). Results of the chemical composition analysis at various points a, b, e of the interrod space in region 3 (Fig. 4) are collected in Table 1 and show a homogeneous composition (within the accuracy limits of the measurements) of the (U, Zr)O_{2-x} ceramic phase (see Ref. [10]; fig. 51 on p. 239, fig. 52 on p. 240 and fig. 55, p. 243). The absence of diffusion profiles in the spatial distribution of the U and Zr components proves that the (Zr, U, O) metal phase is well mixed in the course of high-temperature interactions (oxidation and dissolution) owing to temperature and density variations of the melt (see Ref. [11]).

Table 1
Quantitative results of SEM/EDX analysis of material chemical composition at different locations at elevation 605 mm (position #3 of cross section #k, Fig. 4) of the CORA-W2 test bundle (from Ref. [10], fig. 51, p. 239; fig. 52, p. 240 and fig. 55, p. 243)

Element	Location a	Location b	Location e
O (at.%)	66.7	65.1	66.3
Zr (at.%)	25.4	27.3	25.3
U (at.%)	7.1	7.6	8.4

(4) In the lower part of the bundle, the formation of blockages occurs at a late stage of the relocation process owing to quick cooling of the system (when electrical heating of rod simulators is switched off) and refreezing of the molten metal phase. For this reason, the oxygen content of the melt is comparatively small (Fig. 5) and dendritic ceramic precipitates formed on cool-down are homogeneously distributed in the α-Zr(O) matrix. The main product of the liquid metal (Zr, U, O) phase oxidation is a rather uniform oxide scale ZrO_2 observed on the lateral surface of the solidified melt (Fig. 5).

A generalization of the all above-presented observations and conclusions on the behavior of the molten materials finally results in the following qualitative picture of the mechanical and physico-chemical behavior of the relocating (Zr, U, O) melt.

At the initial stage of the core degradation process the molten materials begin to flow down from some upper hot elevation in the form of separate drops and rivulets and stop at some lower (and colder) elevation. The possible reason of this stopping is cooling down of the drop. Due to deviations of the U–Zr–O composition from the exact eutectic point, the cooling down of the melt leads to a solid fraction formation in some temperature interval $[T_{sol}, T_{liq}]$ and thereby to a steep viscosity increase (up to dozens of times). As a result at some rod elevation where temperature is close to T_{sol}, a viscous mixture slug begins to develop which may form a partial blockage of the coolant channel.

Physico-chemical interactions of the slug materials with steam (as well as of the neighboring Zr cladding material heated by the relocated hot slug, and for this reason intensively oxidized [6]) leads to the heat generation and heating up of the slug. This, in turn, leads to a decrease of the solid fraction and viscosity and a begin of flowing down to the lower (and colder) elevations, resulting in

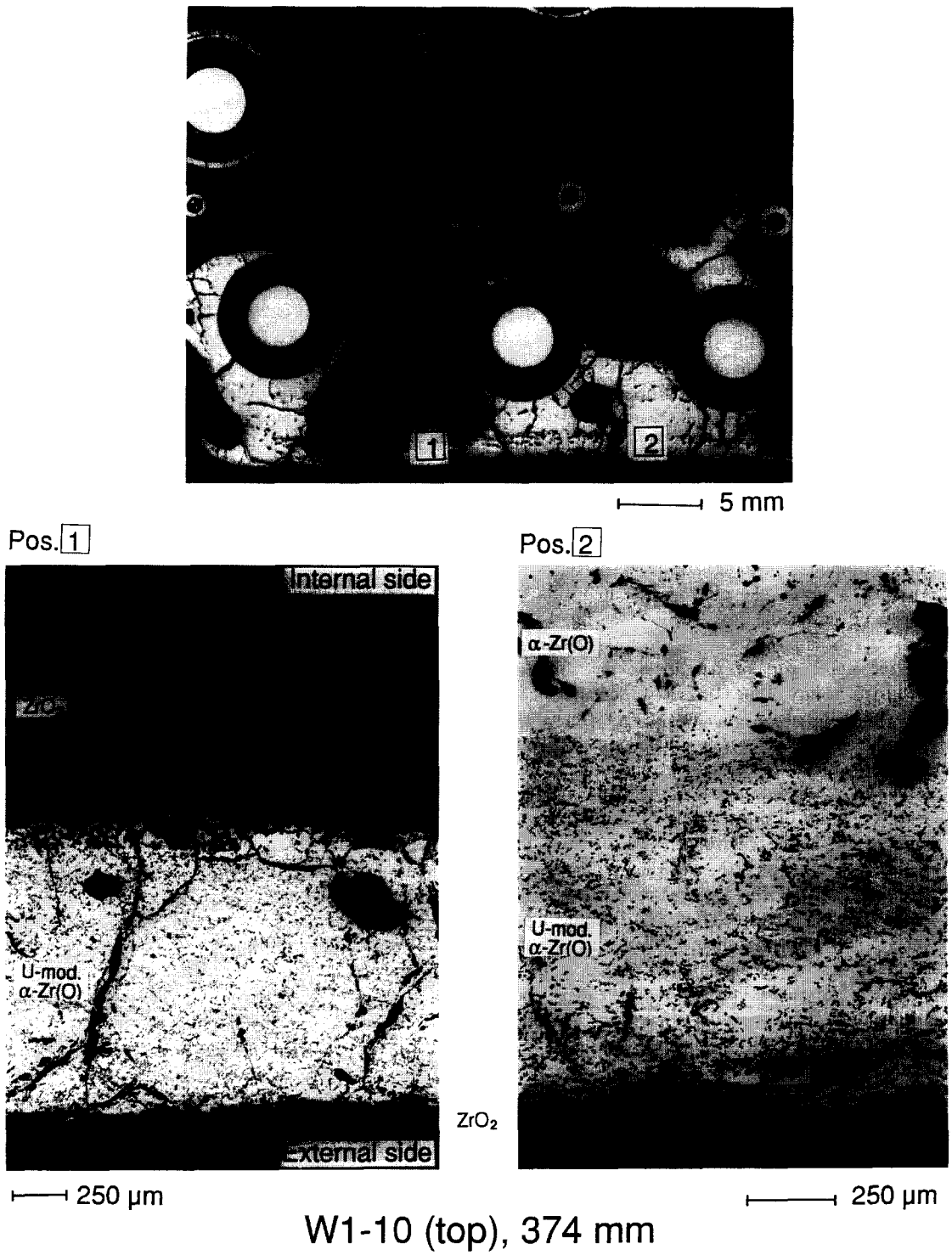

Fig. 5. Cross-section W1-10 (top) of the CORA-W1 test bundle (elevation 374 mm) (from Ref. [5]).

continuous slow relocation of the slug coherently with the temperature front.

During the slug motion the mass exchange process including the mass income from the hot upper elevations in the form of drops, dissolution of the cladding and possible mass outcome occurs from the slug of some hot

portions of the mixture (mainly of metal composition). The mass balance of these processes leads to accumulation of hot molten material ($T \approx 2000$°C) in the interrod space regions in the form of molten pool(s), gradually expanding in the course of further melt accumulation. A relatively thin viscous two-phase layer (crust) formed by the slug at the bottom of the melt along the steep temperature gradient (in the temperature interval $[T_{sol}, T_{liq}]$), supports the molten mass and prevents it from quick falling down.

Rapid processes of drop-like income from above and outcome to below take place against the background of the slow relocation of the molten mass coherent with the underlying slug (crust) motion. This slow relocation makes the main contribution to the axial mass transfer and correlates with the downward propagation of the high-temperature front.

The (Zr, U, O) melt (convectively stirred inside the molten pool) dissolves UO_2 pellets and ZrO_2 cladding scales and is simultaneously oxidized by steam. These chemical processes lead to the growth of the ZrO_2 oxide film on the lateral surfaces of the molten mass and simultaneously to the precipitation and growth of (U, Zr)O_{2-x} ceramic particles in the bulk of the mass (in accordance with the kinetic model developed in Part I).

Correspondingly, it can be assumed that the effective viscosity of the molten mass gradually increases in the course of the ceramic precipitates growth leading to an increase of the solid fracture amount in the bulk of the melt. This additionally (to the underlying crust) prevents the molten mass from quick downward relocation and periodically leads to local captures of the melt in the interrod space (when the amount of solid fracture in the melt becomes sufficiently large). In the course of its further oxidation leading to the formation of the uniform (U, Zr)O_{2-x} ceramic phase areas, the captured material forms local ceramic blockages (debris) at various elevations as observed in the CORA post-test examinations (see point 2 above).

4. Quantitative evaluation of the main processes

As demonstrated above, the molten material apparently accumulates in the steady stage of the melt relocation process in the form of the molten mass which slowly propagates downward. The average velocity of the molten mass motion is apparently determined by a kind of thermal balance between the heat generation due to oxidation and the heat losses due to surrounding rods heating up and the metal cladding dissolution. Quantitative estimations of the energy balance of various processes providing downward propagation of the molten mass with a certain velocity ($v_1 \approx 1$ mm/s), must confirm the self-consistency of the above presented qualitative picture within the accuracy limits of the given estimation approach (i.e. within the accuracy limits of approximately one order of magnitude). More accurate results can be obtained only in the framework of a more strict quantitative theory. It is assumed that after implementation of the developed kinetic model of material interactions (presented in Part I) in severe accident integral codes (simulating core degradation processes) and its coupling with the modified melt relocation model on the basis of the physical mechanisms presented here (see Section 5), a consistent quantitative description of the mechanical and physico-chemical behavior of the relocating melt will be attained.

Therefore, the main task of the present section is to demonstrate that large heat losses at the melt propagation front due to the melting of Zr metal cladding and heat transfer (into the metal cladding, fuel pellets and steam environment) can be compensated by the heat generation in the molten mass due to the melt oxidation (i.e., Stefan's heat balance equation at the propagating front is valid).

In order to estimate heat fluxes at the melt progression front necessary for the cladding melting through, it should be noticed that the cross-section of the metal cladding makes up only a minor part of the melt progression front. In the steady stage of the melt relocation process when lateral expansion of the molten mass becomes significant (and its cross-section comparable with that of the whole bundle), the ratio of the total cross-section of the melting cladding (S_{cl}) to that of the molten mass ($S_0 - S_{UO_2}$) can be roughly estimated as $S_{cl}/(S_0 - S_{UO_2}) \approx 0.2$.

The heat of fusion of Zr is $H_m \approx 22.5$ kJ/mol [12], the molar Zr density is $\rho_{Zr} \approx 0.06$ mol/cm^3. Therefore, the balance of heat fluxes through the unit surface of the molten mass bottom which sustains the melt progression front velocity $v_1 \approx 1$–2 mm/s must coincide with the surface heat sink:

$$Q_m \approx H_m \rho_{Zr} v_1 S_{cl}/(S_0 - S_{UO_2}) \approx 50 \text{ W/cm}^2. \quad (1)$$

The heat conduction flux Q_c to the metal cladding at the front can be evaluated from the axial temperature gradient below the front (estimated from Fig. 1 as $\nabla T \approx 50$–80 K/cm) and the thermal conductivity of Zr (extrapolated to $T \approx 2000$°C from the lower temperature data [13], $\chi \approx 40$ W/m K):

$$Q_c \approx \chi \nabla T \approx 20 \text{ W/cm}^2. \quad (2)$$

The heat flux through the remaining part of the melt progression front is provided by steam convection and irradiation from the surface.

In order to make a conservative estimation for the heat losses it can be proposed that the heat flux through the unit square of this part of the surface does not exceed the value Q_c. Therefore, from Eqs. (1) and (2) the heat flux matching condition at the front takes the following form:

$$Q_0 = Q_c + Q_m \approx 70 \text{ W/cm}^2, \quad (3)$$

where Q_0 describes the heat flux from the molten phase in the axial direction (Fig. 6). The main source of this heat

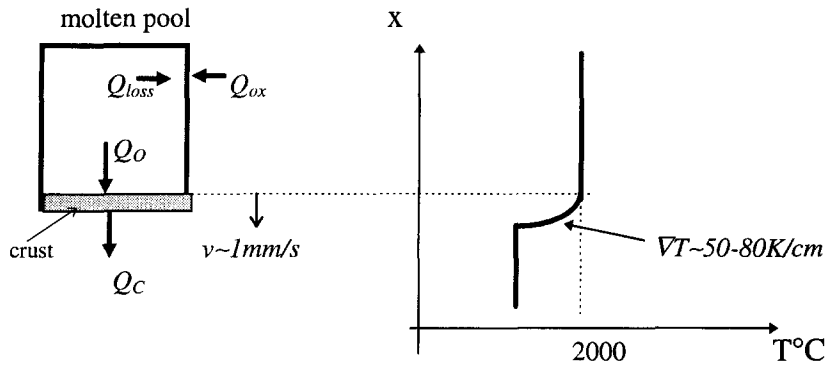

Fig. 6. Schematic representation of the heat fluxes through the surfaces of the relocating melt.

flux Q_0 is the heat generation due to oxidation of the melt. It can be demonstrated here that this source can be large enough to provide the propagation of the melt front with the observed velocity $v_1 \approx 1$ mm/s, i.e. the validity of the flux matches, Eq. (3).

In order to estimate the value of this heat source, it should be noticed that the characteristic thickness of the oxide scale formed at the lateral surface of the molten mass can be roughly evaluated from the above-presented figures as ≈ 200–400 μm. The diffusion coefficient of oxygen in the ZrO_2 phase is $D \approx 9 \times 10^{-4}$ cm^2/s at $T \approx 2000$°C, the concentration drop across the scale $\Delta c \approx 0.094(1 - x/2)$ mol/cm^3, where $x \approx 1.85$ in accordance with the equilibrium phase diagram [14] at this temperature, therefore, the oxygen diffusion flux can be estimated as $J \approx (1.5\text{–}3) \times 10^{-4}$ mol/cm^2 s. Since the heat of oxidation of Zr is $H_{ox} \approx 300$ kJ/mol [15], the heat flux from the lateral surface into the molten mass is estimated as

$$Q_{ox} \approx H_{ox} J \approx 50\text{–}100 \text{ W/cm}^2. \quad (4)$$

It is more complicated to evaluate the oxidation of the upper surface of the molten pool, since no traces of horizontal thin ZrO_2 oxide layers were detected in the post-test cross-sections of the CORA bundle. Nevertheless, it can be logically proposed that the upper oxide scale grows coherently with relocation of the molten mass (with the velocity v_1), periodically loosing contact and separating from the moving melt, collapsing and growing again. The time of 'separation' τ of the diffusionally growing oxide scale can be estimated from the relation $(D\tau)^{1/2} \simeq v_1\tau$, i.e. $\tau \simeq 10^{-1}$ s, therefore, a mean steady thickness of the oxide layer $d \simeq (D\tau)^{1/2} \simeq 100$ μm is comparable with the thickness of the observed lateral scale.

Additional reasons for the stabilization or very slow variation of the oxide scale thickness in the course of the molten pool oxidation (accompanied by precipitation of the (U, Zr)O_{2-x} ceramic phase in the bulk of the melt) are presented in Part I.

Therefore, the presented semi-quantitative estimations show that the heat fluxes $Q_{ox} \approx 50$–100 W/cm^2 from the lateral and upper surfaces into the molten mass which are partially compensated by the heat losses from these surfaces due to irradiation, steam convection and heating of the surrounding pellets ($Q_{loss} \leq 20$ W/cm^2, as conservatively estimated above) can counterbalance the heat flux Q_0 from the molten mass through the melt progression front and thus, confirm the validity of Eq. (3), which provides the observed propagation velocity of this front $v_1 \approx 1$–2 mm/s.

5. Discussion

This last conclusion seems to be especially important for the quantitative modeling of the melt progression within the framework of the integral codes, since it demonstrates that in the steady state of the process the molten mass propagation velocity practically does not depend on the droplets dynamics and is determined predominantly by the heat balance at the melt progression front. In particular this consideration apparently explains the existence of the abrupt temperature drop at the front during all the steady stage of the relocation process (see Fig. 1), which unavoidably should be 'washed out' in the opposite case of separate relocations of droplets and rivulets.

In order to clarify this physical picture, a simple analogy of the studied process with downward propagation of the flame front in a burning candle can be derived (see schematic representation in Fig. 7). In both cases the fusion front at the bottom of the molten pool determines relocation dynamics of the major part of the melt, whilst separate droplets and rivulets play only a minor role in the general picture of the relocation process. For these reasons, the relocation velocity of the fusion front in both the cases can be roughly determined from the heat flux matches at this front and the latent heat of fusion of the solid material (molten through) (see Eqs. (1)–(3)).

To cover the general description of mass relocation throughout the whole course of an accident, one has to consider both massive melt (slug) and drops/rivulets

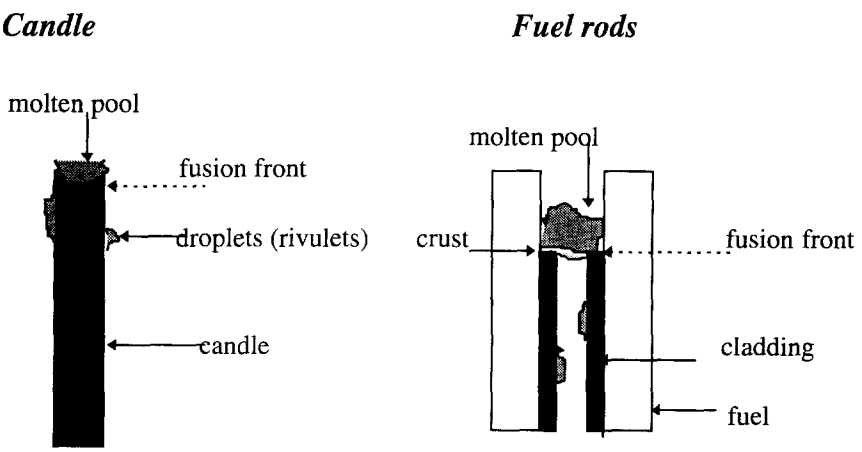

Fig. 7. Schematic representation of the analogy between two 'candling' processes.

modes of the candling process. For modeling of the collective effects (confluence of several drops in a slug; mass income and outcome) it is necessary to solve the equations of motion of a liquid element with account of locations and motion of other liquid elements, i.e. drops cannot be considered independently.

The other important point is the steep increase of the melt viscosity due to precipitation and growth of (U, Zr)O_{2-x} ceramic particles in the bulk of the metallic melt in the course of the oxidation. It is just this effect which leads to the slow (as compared with drops and rivulets) molten mass (slug) relocation. Indeed, owing to the melt viscosity increase, a 'critical dimension' of a liquid droplet (and/or rivulet) also increases which determines the cessation of its relocation along the vertical rod surface [16]. As soon as this critical dimension exceeds the interrod distance, relocations of separate droplets and rivulets cease, and the molten pool accumulation and slug formation starts.

Cladding and pellets dissolution by the slug, the slug oxidation by steam, as well as the mass income from above and outcome to below, change the chemical composition of the slug. On the other hand, the solid fraction value and also the rates of the dissolution and oxidation reactions will depend on the current chemical composition of the slug. For self-consistent modeling of these processes it is necessary to calculate the chemical composition of the slug current by the solution of the separate mass balance equations for each chemical component.

6. Conclusions

On the basis of thorough analysis of metallographic post-test examination data obtained in the fuel bundle CORA experiments, investigations and modeling of high-temperature processes are presented which are associated with the oxidation of U–Zr–O molten mixtures under various conditions of severe accidents (intact heated fuel rods, considered in Part I, or relocating melt).

In Part II qualitative results on the nature of Zr-rich melt oxidation and interactions with fuel rods obtained in Part I, allow further interpretation of the post-test examinations of structures formed in the tests CORA-W1 and CORA-W2 under more complicated conditions, namely during downward relocation of the melt. On the basis of these analyses, on the one hand, and from the comparison of time behavior of high-temperature curves with visual observations of the melt propagation front, on the other hand, it is concluded that the major part of molten cladding material relocates downward in the form of a massive slug very slowly in comparison with rather quick relocations of separate drops and rivulets. During this slow downward propagation the slug accumulates fresh portions of molten cladding, extensively oxidizes and simultaneously dissolves UO_2 pellets and ZrO_2 scales of the cladding. Analysis of these simultaneous physico-chemical processes by the kinetic oxidation/dissolution model developed in Part I of the paper, allows the explanation of reasons for the observed rather low velocity of slug relocation (owing to precipitation of the ceramic (U, Zr)O_{2-x} phase in the course of oxidation/dissolution and as a result, strong increase of the effective viscosity of the molten slug) and rather high heat generation provided cladding fusion and heating of the surrounding materials in the course of slug relocation. The presented semi-quantitative estimations show that the heat fluxes into the molten mass induced by the melt oxidation and partially compensated by the heat losses from the melt surfaces due to irradiation, steam convection and heating of the surrounding pellets can counterbalance the heat flux from the molten mass through the melt progression front. This confirms the validity of Stefan-type flux matches at the front, which provides the observed low propagation velocity of this front ($v_1 \approx 1$ mm/s in the CORA-W1 test). On the basis of these analyses, the necessity of the further modification of relo-

cation models for description of relocation of molten slugs (rather than drops, rivulets or films), and coupling of the modified models with the oxidation/dissolution model (developed in Part I) for the self-consistent description of oxidation during melt relocation within the framework of integral codes, is revealed.

Acknowledgements

The authors are grateful to Dr P. Hofmann and Dr V. Noack (FZK, Karlsruhe) for valuable discussions and comments. We also thank them and Dr S. Hagen (FZK, Karlsruhe) for their kind delivery of the original photographs of samples from the CORA tests. This work was supported by the US Nuclear Regulatory Commission under the NRC Contract No. W6452.

References

[1] T.J. Haste, B. Adroguer, U. Brockmeier, P. Hofmann, K. Mueller, M. Pezzilli, In-Vessel Core Degradation in LWR Severe Accidents, Report EUR 16695 EN, 1996.

[2] M. Firnhaber, L. Yegorova, U. Brockmeier, S. Hagen, P. Hofmann, K. Trambauer, OECD/NEA-CSNI International Standard Problem ISP36, CORA-W2 Experiment on Severe Fuel Damage for a Russian Type PWR, Comparison Report, GRS-120, FZKA 5711, OCDE/GD(96)19, ISBN 3-923875-81-9, 1996.

[3] S.R. Kinnersly, J.N. Lillington, A. Porracchia, K. Soda, K. Trambauer, P. Hofmann, Y. Waarenpera, R.A. Bari, C.E.L. Hunt, J.A. Martinez, In-Vessel Core Degradation in LWR Severe Accidents: A State-of-the-Art Report to CSNI, Jan. 1991, NEA/CSNI/R(91)12, 1991.

[4] P. Hofmann, S. Hagen, V. Noack, G. Schanz, G. Schumacher, L. Sepold, Kerntechnik 59 (1994) 197.

[5] S. Hagen, P. Hofmann, V. Noack, G. Schanz, G. Schumacher, L. Sepold, Test Results of Experiment CORA W1, Report KfK 5212, 1994.

[6] V. Noack, S. Hagen, P. Hofmann, G. Schanz, L. Sepold, Nucl. Technol. 117 (1997) 158.

[7] W. Hering, Modellierung des Experimentes CORA und Interpretation von Versuchsergebnissen mit dem Erweiterten Kernschmelzcode SCDAP/MOD1, thesis, 1993.

[8] W. Dienst, P. Hofmann, D. Kerwin-Peck, Nucl. Technol. 65 (1984) 109.

[9] S. Hagen, P. Hofmann, V. Noack, G. Schanz, G. Schumacher, L. Sepold, Results of Experiment CORA W2, Report KfK 5363, 1994.

[10] L. Sepold (Ed.), Post-test Examination of the VVER-1000 Fuel Rod Bundle CORA-W2, FZKA 5570, 1995.

[11] M.S. Veshchunov, P. Hofmann, A.V. Berdyshev, J. Nucl. Mater. 231 (1996) 1.

[12] D.R. Olander, Wei-E. Wang, J. Nucl. Mater. 247 (1997) 258.

[13] J.K. Fink, L. Leibowitz, J. Nucl. Mater. 226 (1995) 44.

[14] J.P. Abriata, J. Garces, R. Versaci, Bull. Alloy Phase Diagrams 7 (1986) 116.

[15] D.R. Olander, J. Electrochem. Soc. 131 (1984) 2161.

[16] A.V. Palagin, On the flowing down the fuel rod of Zr–U–O liquefied mixture during severe accident at nuclear power plant, Preprint NSI-1-93, Moscow, 1993.